

SCIENTIFIC REPORTS



OPEN

Embryonic/fetal mortality and intrauterine growth restriction is not exclusive to the CBA/J sub-strain in the CBA × DBA model

Received: 22 April 2016
Accepted: 19 September 2016
Published: 21 October 2016

Kelly J. McKelvey^{1,2}, Vanessa M. Yenson^{1,2}, Anthony W. Ashton^{1,2}, Jonathan M. Morris^{1,2,3} & Sharon A. McCracken^{1,2}

Inbred strains of mice are powerful models for understanding human pregnancy complications. For example, the exclusive mating of CBA/J females to DBA/2J males increases fetal resorption to 20–35% with an associated decline in placentation and maintenance of maternal Th1 immunity. More recently other complications of pregnancy, IUGR and preeclampsia, have been reported in this model. The aim of this study was to qualify whether the CBA/CaH substrain female can substitute for CBA/J to evoke a phenotype of embryonic/fetal mortality and IUGR. (CBA/CaH × DBA/2J) F1 had significantly higher embryonic/fetal mortality ($p = 0.0063$), smaller fetuses ($p < 0.0001$), and greater prevalence of IUGR ($< 10^{\text{th}}$ percentile; 47% vs 10%) than (CBA/CaH × Balb/c) F1. Placentae from IUGR fetuses from all mating groups were significantly smaller ($p < 0.0001$) with evidence of thrombosis and fibrosis when compared to normal-weight fetuses ($> 10^{\text{th}}$ percentile). In addition, placentae of “normal-weight” (CBA/CaH × DBA/2J) F1 were significantly smaller ($p < 0.0006$) with a greater proportion of labyrinth ($p = 0.0128$) and an 11-fold increase in F4/80 + macrophage infiltration ($p < 0.0001$) when compared to placentae of (CBA/CaH × Balb/c) F1. In conclusion, the embryonic/fetal mortality and IUGR phenotype is not exclusive to CBA/J female mouse, and CBA/CaH females can be substituted to provide a model for the assessment of novel therapeutics.

In the last century there has been a vast improvement in overall perinatal health. However, high rates of perinatal mortality and morbidity persist in spite of advances in medical technologies and management, such as routine use of ultrasound to monitor fetuses during pregnancy. An important cause of perinatal mortality, secondary only to preterm birth, is the failure of the fetus to reach its growth potential *in utero*, termed intrauterine growth restriction (IUGR); defined by the World Health Organisation as an estimated fetal weight below the 10th percentile of the recommended gender-specific birth weight for gestational age reference curve¹. Worldwide, IUGR affects 7–15% of pregnancies^{2,3} and has an 8–10-fold greater risk of perinatal mortality when compared to pregnancies with a normal-weight fetus⁴.

Mouse models are a powerful tool for understanding pregnancy outcomes, as well as embryonic and placental growth and development. Mice and humans share physiological characteristics during both healthy pregnancy and those with adverse outcomes including immunological, hormonal, and fetal/placental development. While animal models created by genetic, surgical and pharmacological manipulation are highly valuable for studying the pathogenesis of IUGR, these models inadvertently introduce confounding factors when utilised for the assessment and development of new therapeutics. In contrast, the CBA/J × DBA/2J murine model⁵ spontaneously develops IUGR and embryonic/fetal mortality^{6,7} and shares features of the human IUGR complication, including inadequate maternal arterial remodelling at the implantation sites^{8,9} and utero-placental dysregulation with complement deposition on trophoblasts, increased inflammatory cell infiltration (neutrophil and monocyte) and tumour necrosis factor (TNF)- α expression in maternal decidua^{6,10,11}.

¹Division of Perinatal Medicine, Kolling Institute, Northern Sydney Local Health District, St Leonards, 2065 NSW, Australia. ²Sydney Medical School Northern, University of Sydney, St Leonards, 2065 NSW, Australia. ³Department of Obstetrics and Gynaecology, Royal North Shore Hospital, Northern Sydney Local Health District, St Leonards, 2065 NSW, Australia. Correspondence and requests for materials should be addressed to K.J.M. (email: kelly.mckelvey@sydney.edu.au)

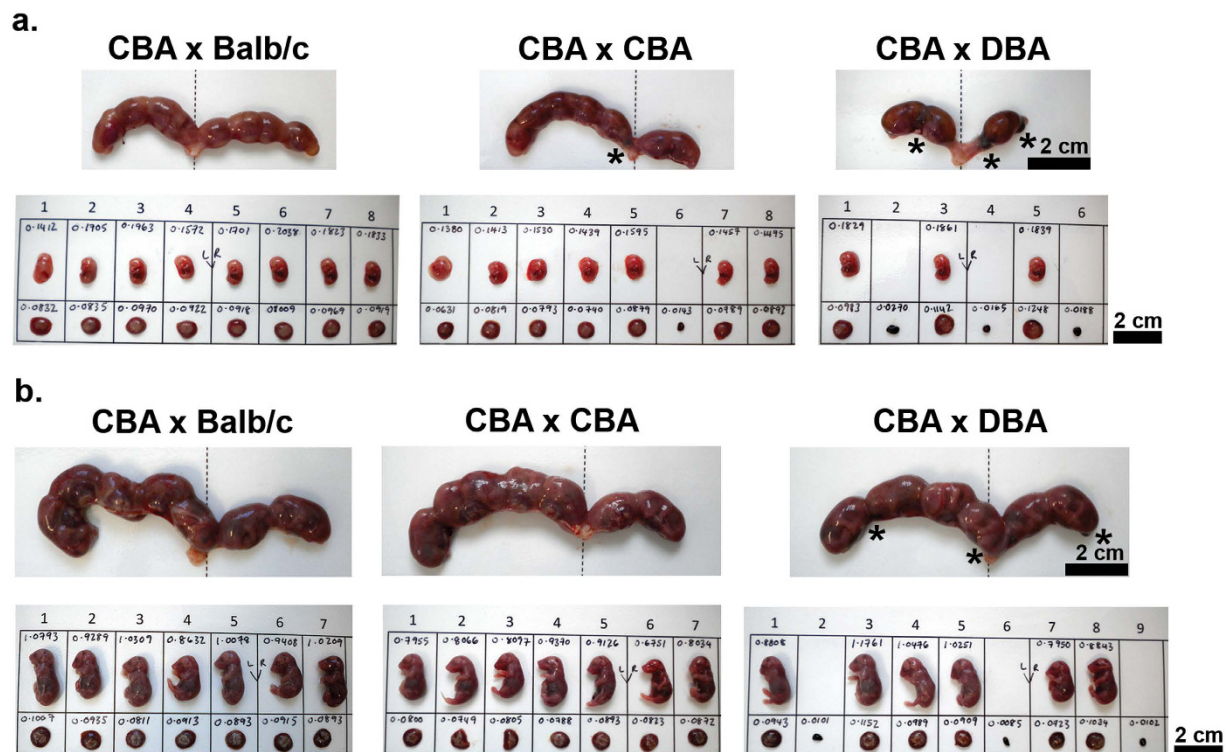


Figure 1. Macroscopic pregnancy outcomes of murine CBA/CaH × DBA/2J pregnancies. Representative photographs of gravid uteri harvested from CBA/CaH × Balb/c, CBA/CaH × CBA/CaH and CBA/CaH × DBA/2J pregnancies at (a) 14.5 dpc (N = 20 dams per strain) and (b) 18.5 dpc (N = 30 dams per strain). Fetuses and placentae were excised, measured, weighed and photographed. Weights of fetuses, placentae and resorptions are indicated in grams. Asterisks denote resorption sites indicating embryonic/fetal mortality.

Since identification of the abortion-prone phenotype in pregnant DBA/2J-mated CBA/J female mice in 1980, subsequent studies reported that this phenotype is exclusive to the American Jackson Laboratory-derived CBA/J female, with other CBA sub-strains (CBA/Ca, CBA/JHan, CBA/N) showing normal incidence^{12,13}. This was believed to arise from semi-allogeneic rejection of the placenta by maternal immune cells due to differences in the murine major histocompatibility antigen, termed H-2 antigens which have accumulated by the separate breeding lines since 1935^{13,14}; CBA/J (*H2k, Mlsd*) and CBA/Ca and CBA/N (*H2k, Mlsb*). However, ‘genetic drift’ may, in part, explain why more recent papers have identified new phenotypes in the CBA/J × DBA/2J model including fetal growth restriction⁶ and immunologically-mediated pre-eclampsia at mid gestation (15.5 dpc)^{7,15}, though neither phenotype has been replicated in a term population (17.5–18.5 dpc)¹⁶.

As CBA/J mice are not currently available in Australia, and CBA/J and CBA/CaJ mice show differences in aging phenotypes¹⁷ we examined whether the Commonwealth-derived CBA/CaH.Arc mouse (Animal Resource Centre, Murdoch, Australia) can substitute for the American-derived CBA/J sub-strain in the spontaneous CBA × DBA/2J murine model. In this study we show that the CBA/CaH pregnant female develops an IUGR and embryonic/fetal mortality phenotype at mid-gestation (14.5 dpc) following allogeneic mating with DBA/2J males, suggesting that this sub-strain can be substituted where CBA/J mice are not available.

Results

To establish whether CBA/CaH × DBA/2J pregnancies show the same propensity for embryonic/fetal mortality and IUGR as CBA/J females, 150 CBA/CaH females were placed with DBA/2J, Balb/c or CBA/CaH males overnight. Both mid-gestation (14.5 dpc, n = 20 matings per group) and term (18.5 dpc, n = 30 matings per group) time points were assessed to directly compare the fetal outcomes. Harvesting of gravid uteri, including the cervix, revealed the presence of resorption sites but showed no macroscopic uterine abnormalities in CBA/CaH × DBA/2J pregnancies at mid-gestation (Fig. 1a) or term (Fig. 1b).

Embryonic/fetal mortality is increased in CBA/CaH × DBA/2J pregnancies. The severest form of IUGR in our cohort is reflected as embryonic/fetal mortality (resorption). Overall, there was a significant increase in (CBA/CaH × DBA/2J) F1 embryonic/fetal mortality in when compared to (CBA/CaH × Balb/c) F1 at term ($21.1 \pm 2.4\%$ vs $10.7 \pm 2.9\%$, $p = 0.0079$; Fig. 2a), while mid-gestation did not reach significance ($22.6 \pm 3.89\%$ vs $8.5 \pm 5.89\%$, $p = 0.1569$). Mortality in the (CBA/CaH × DBA/2J) F1 ranged widely from 0 to 63.4% at mid-gestation and between 0 to 55.5% in term populations, indicating that not all pregnancies are affected. This was particularly evident at term with 86.7% of CBA/CaH × DBA/2J litters containing resorptions, compared to 45.8% CBA/CaH × Balb/c and 79.2% for CBA/CaH × CBA/CaH pregnancies ($X^2 = 11.91$, $p = 0.0026$). There was no statistical difference at mid-gestation.

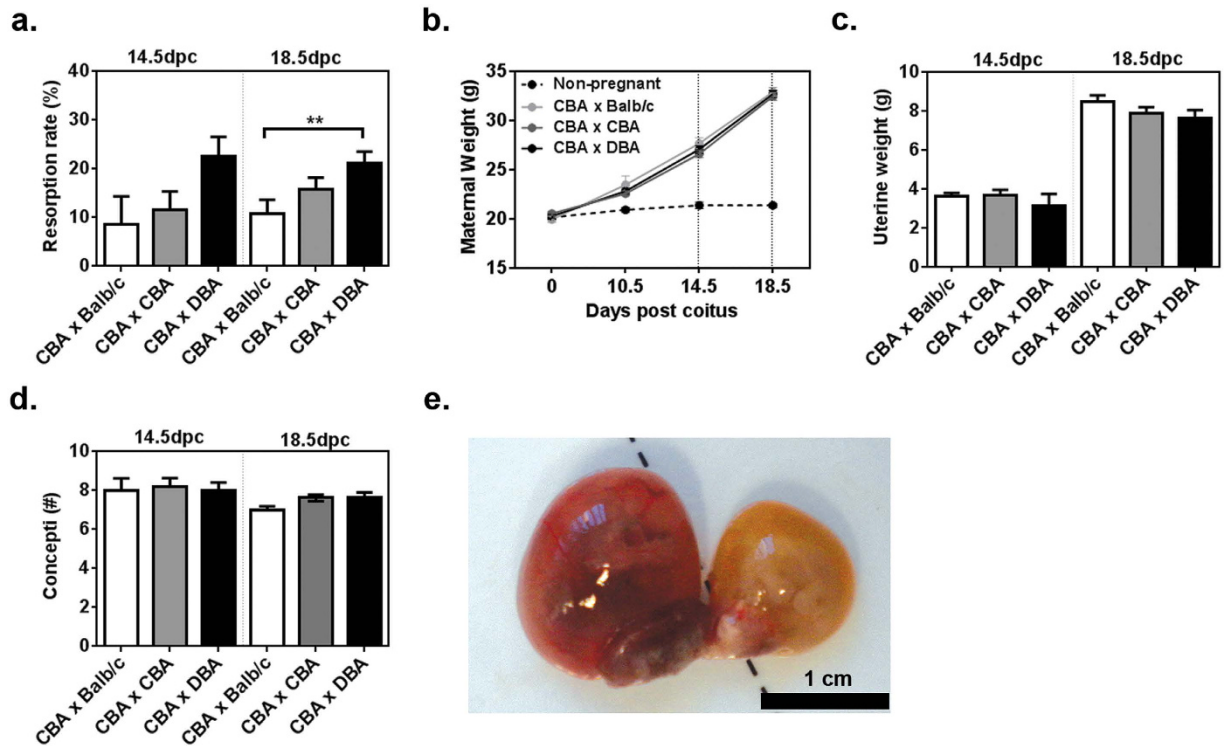


Figure 2. Maternal characteristics of the murine CBA/CaH \times DBA/2J pregnancies. (a) Embryonic/fetal mortality (resorption) rate, (b) maternal body weight at mating, (c) uterine wet weight, and (d) number of concepti at 14.5 dpc (N = 20 dams per strain) and 18.5 dpc (N = 30 dams per strain). (e) Representative photograph of asymmetrical diamniotic/dichorionic (placentally fused) twins. All data are represented as mean \pm SEM. ** $p < 0.01$ vs value for CBA \times Balb/c by One-way ANOVA with Tukey's multiple comparison test.

Descriptors of the progression of resorption are 'embryonic', 'bag of cells' and 'clot' phases¹⁸, reflecting progressive loss of the fetal and placental structures via aseptic intravital autolysis. In our study evidence of all three stages was present, irrespective of the group analysed, with the clot phase most common in mid-gestation (70/72, 97.2%) and term (84/96, 87.5%) pregnancies. Embryonic phase resorptions were observed at term (6/96, 6.3%), but not mid-gestation, and were primarily associated with (CBA/CaH \times Balb/c) F1 potentially indicating that fetal death and resorption takes place at a later time point in these pregnancies.

A range of factors have been found to influence embryonic/fetal mortality in mice and specifically the CBA/J \times DBA/2J murine model. These include maternal nutrition, primigravidity, immunological environment, maternal age and overcrowding of one uterine horn^{19,20}. However, irrespective of time-point we found no differences in maternal weight gain, uteri wet weight, or total number of concepti when compared to CBA/CaH \times Balb/c (Fig. 2). The number of concepti in left vs right uterine horns of CBA/CaH \times DBA/2J pregnancies was uneven (≥ 2 concepti difference between left and right horns; $X^2 = 7.370$, $p = 0.0251$) when compared to CBA/CaH \times Balb/c, but the 'overcrowded' horn was not associated with greater mortality when compared to the 'uncrowded' horn ($X^2 = 2.249$, $p = 0.3248$; and shown Fig. 1).

While mortality rates did not differ, we considered whether CBA/CaH \times DBA/2J pregnancies have abnormal spacing between implantation sites which may impact placental development leading to the increased mortality we observed. Using the incidence of diamniotic/dichorionic (placentally-fused) twins as a surrogate for abnormal implantation site, at term the incidence of twins was 3.6% (6/168) in (CBA/CaH \times Balb/c) F1, 2.2% (4/183) in (CBA/CaH \times CBA/CaH) F1, and 3.5% (8/230) in (CBA/CaH \times DBA/2J) F1 and not statistically significant ($X^2 = 0.7434$, $p = 0.6895$). Of the observed twin fetuses 50%, 25% and 25% respectively were asymmetrical (different size fetuses; example shown in Fig. 2e). At mid-gestation only one instance of diamniotic/dichorionic twins was observed in a CBA/CaH \times DBA/2J pregnancy. These data suggest that overcrowding, with or without abnormal spacing, was not a significant contributing factor to the increased embryonic/fetal mortality observed in (CBA/CaH \times DBA/2J) F1 and (CBA/CaH \times CBA/CaH) F1.

Proportion of IUGR fetuses is increased in CBA/CaH \times DBA/2J pregnancies. Studies using the CBA/J \times DBA/2J murine model have reported that surviving fetuses show consistent and significant 'IUGR'⁶, based on a statistical reduction in average fetal weight. To utilise a biologically relevant criterion for IUGR, we quantified the prevalence of IUGR in our murine pregnancies using the human clinical definition of $< 10^{\text{th}}$ percentile for gestational age, with fetuses from allogeneic (CBA/CaH \times Balb/c) F1 as the population standard. Fetal wet weight and crown-rump length (CRL)²¹ were assessed and demonstrated a strong correlation at both time points (14.5 dpc $r = 0.77$ to 0.89 ; $p = 0.0406$ to $p < 0.0001$; and 18.5 dpc $r = 0.91$ to 0.94 , $p < 0.0001$ Fig. 3a).

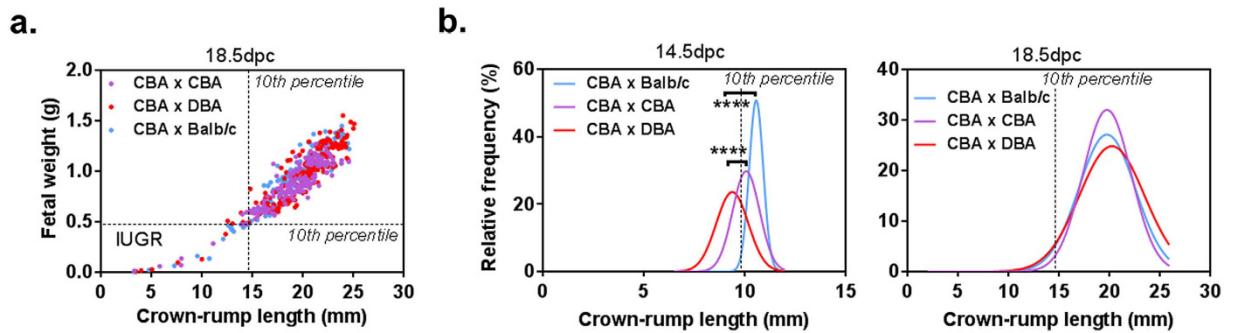


Figure 3. Fetal characteristics of the murine CBA/CaH \times DBA/2J model. Fetuses were excised from gravid uteri at 14.5 and 18.5 dpc. (a) Crown-rump length showed a strong positive correlation with fetal wet weight. (b) Distribution of fetal crown-rump length for all strains where a length $< 10^{\text{th}}$ percentile of (CBA \times Balb/c) F1 were denoted as intrauterine growth restricted (IUGR; b). *** $p = 0.005$. **** $p < 0.0001$ vs (CBA \times Balb/c) F1 by One-way ANOVA with Tukey's multiple comparison test.

Using our definition, IUGR fetuses were denoted as those with a wet weight $< 0.1427\text{g}$ and $< 0.4725\text{g}$ and/or CRL $< 9.75\text{ mm}$ and $< 14.75\text{ mm}$ at 14.5 and 18.5 dpc, respectively. At mid-gestation, 47% of (CBA/CaH \times DBA/2J) F1 fell below the 10^{th} percentile confirming a substantial IUGR phenotype at this time point (Fig. 3b). From 20 pregnant dams this equated to 46 IUGR fetuses, compared to 31 for (CBA/CaH \times CBA/CaH) F1 and 13 for (CBA/CaH \times Balb/c) F1. The number of IUGR fetuses dropped markedly at term with only 5–6 IUGR fetuses in all pregnancy groups. In contrast, the number of resorptions at term remained high; 46 in (CBA/CaH \times DBA/2J) F1, 24 in (CBA/CaH \times CBA/CaH) F1 and 14 in (CBA/CaH \times Balb/c) F1. We propose that IUGR fetuses present at 14.5 dpc become non-viable by term (present as resorptions) resulting in a 'perceived' absence of IUGR at term in the CBA/CaH \times DBA/2J pregnancies. There is precedence for this, with pregnant mice treated with 6 mg of the yeast extract Malucidin at 16–17 dpc, showing complete resorption of a fetus after 48 hr²². Even in large mammals, such as dogs, complete resorption of a fetus takes only 2–5 days and is preceded by reduced growth and/or development of the embryo and fetus²³.

Placentae from IUGR fetuses show histopathology. Macroscopically, the murine IUGR fetuses were developmentally delayed with smaller, thinner and/or pale placentae in comparison to normal-weight littermates ($> 10^{\text{th}}$ percentile; Fig. 4a). Quantitation of placental characteristics confirmed that IUGR placentae from (CBA/CaH \times DBA/2J) F1 weighed on (mean) average 24% less at mid-gestation ($p = 0.011$) and 47% less at term ($p < 0.0001$) than their normal-weight littermates (Fig. 4b). Representative histological sections of IUGR placentae are shown in Fig. 4c (c.f. normal-weight in Fig. 4e). Evidence of pathological changes including thrombosis and fibrosis were present in placentae from IUGR fetuses of all groups (Fig. 4d), consistent with placental patho-histological observations of human IUGR placentae^{24,25}.

Among the IUGR fetuses of all strains there were no differences in placental dimension at either time point (Table 1). In mice the primary site of feto-maternal exchange is the labyrinth, with the maternal decidua providing anchorage to the uterine wall and the fetal chorionic plate delivering blood to/from the umbilical cord. The proportion of IUGR placentae dedicated to the labyrinth layer was significantly less in (CBA/CaH \times DBA/2J) F1 compared to (CBA/CaH \times CBA/CaH) F1 and (CBA/CaH \times Balb/c) F1 at mid-gestation, but did not reach significance at term (Table 1, and see Fig. 4f for colour rendering of placental layers). The trophospongium and maternal decidua layers were highly variable among the (CBA/CaH \times DBA/2J) F1 cohort at 14.5 dpc indicating there may be a range of dysfunction among the placentae in this cohort (i.e. mild, moderate, severe).

One indicator of placental function, or the efficiency of placental nutrient transport, is the ratio of fetal wet weight to placental wet weight in grams²⁶. In addition, with the placenta acting as a nutrient sensor and storage site for glucose (as glycogen) during pregnancy, we sought to determine whether there are changes in the proportion of glycogen-containing cells, and by extension the energy repository, available for fetal growth and development of (CBA/CaH \times DBA/2J) F1. There was no significant difference in placental efficiency or the proportion of glycogen-containing cells at either time point between the (CBA/CaH \times DBA/2J) F1 and (CBA/CaH \times Balb/c) F1 IUGR placentae, although trends toward reduced efficiency and glycogen storage were present (Table 1). Meanwhile, the IUGR placentae of (CBA/CaH \times CBA/CaH) F1 showed the highest placental efficiency of the three strains (Table 1).

Comparison of placental morphology in IUGR and normal-weight fetuses. Normal-weight data is provided in Table 2 and micrographs in Fig. 4e. The p -values for the statistical comparison between placentae of IUGR and normal-weight fetuses of the same strain are provided in Supplementary Table I. Consistent with reduced placental weight, the IUGR placentae of all strains were significantly smaller in dimension (diameter, thickness and/or cross-sectional midline area) than their normal-weight littermates with the differences more pronounced at term than mid-gestation (Fig. 4a,e, and Supplementary Table I). When compared to normal-weight fetuses at mid-gestation, the placentae of IUGR fetuses from (CBA/CaH \times DBA/2J) F1, but not the other strains, had smaller labyrinth (39.7 vs 52.4%, $p < 0.0001$) and larger trophospongium (41.4 vs 24.7%; $p < 0.0001$) (Supplementary Table I). Combined with the aforementioned analysis of placental structure of

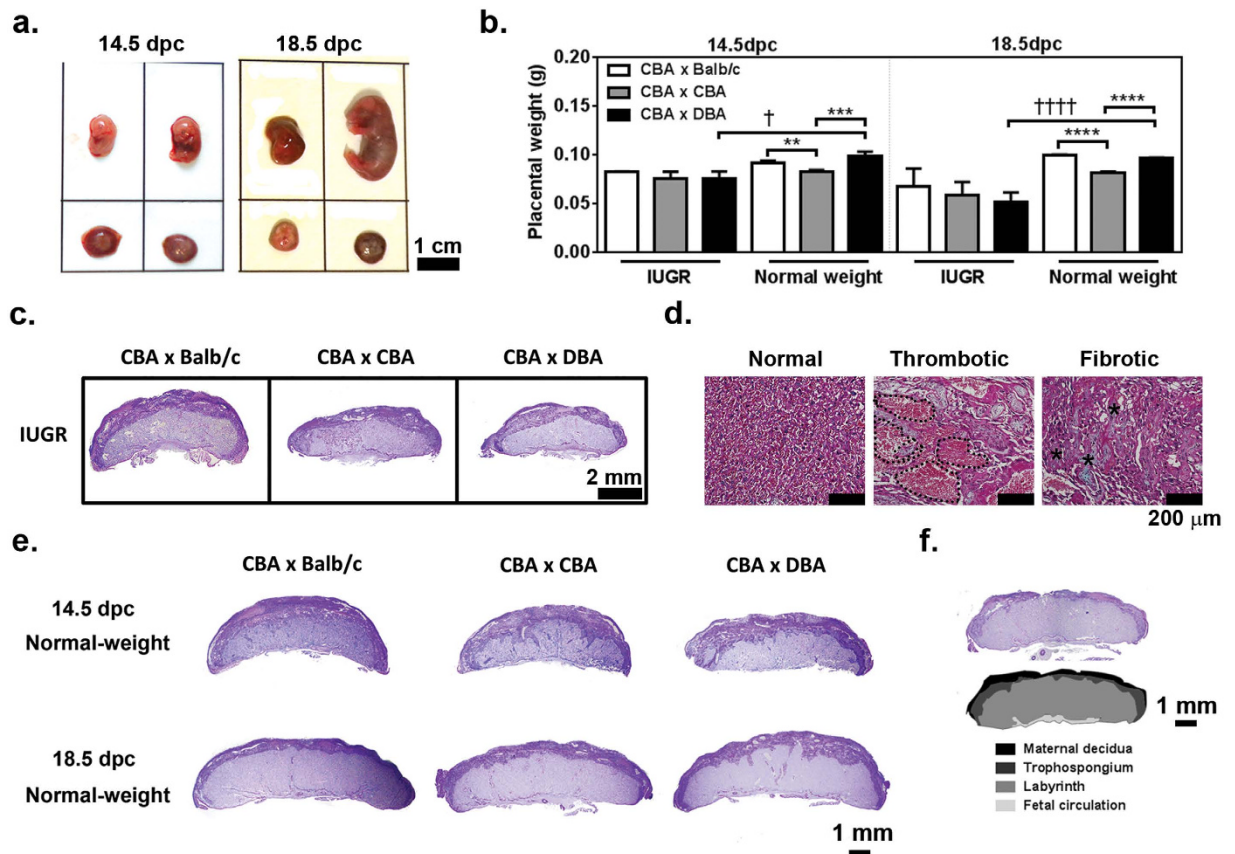


Figure 4. Macroscopic and histological characteristics of murine placentae from IUGR and normal-weight fetuses in the CBA/CaH \times DBA/2J model. (a) Representative photograph of IUGR (<10th %) and normal-weight (>10th %) littermates at 14.5 dpc (left) and 18.5 dpc (right). (b) Placental weight for IUGR and normal-weight fetuses represented as mean \pm SEM. (c) PAS-stained sections of resorptions and placentae from IUGR fetuses (14.5 dpc) were assessed for differences in placental dimensions and the proportion devoted to the labyrinth, trophospongium and maternal decidua. (d) Comparison of normal labyrinthine tissue and areas of thrombotic (dotted line) and fibrotic tissue (asteri; presence of blue/green collagen) from IUGR associated placentae stained with fast-green Masson's trichrome. (e) PAS-stained sections of placentae from normal-weight fetuses at 14.5 and 18.5 dpc, and (f) a (CBA/CaH \times Balb/c) F1 placenta at 18.5 dpc that has been colour rendered to show the placental layers quantitated in Table 2. (b) ** $p < 0.01$, *** $p < 0.001$ vs CBA \times CBA by One-way ANOVA with Tukey's multiple comparison test; [†] $p < 0.05$ vs value for IUGR by unpaired two-tailed Student T test.

IUGR placentae, this may indicate that although each strain has IUGR fetuses, the histopathology of the (CBA/CaH \times DBA/2J) F1 IUGR fetuses is more severe at this time point.

At term all strains demonstrated significantly greater placental efficiency for normal-weight fetuses compared to IUGR (all $p < 0.0001$; Table 1), though only the (CBA/CaH \times Balb/c) F1 IUGR placentae showed differences in placental layer composition compared to normal-weight fetuses; less labyrinth (48.6 vs 63.5%; $p < 0.0001$), and larger trophospongium (29.1 vs 19.8%; $p < 0.0001$), maternal decidua (22.3 vs 16.7%; $p = 0.0004$) and glycogen storage (14.1 vs 9.5%; $p < 0.0001$; Table 1).

Normal-weight fetuses of CBA/CaH \times DBA/2J pregnancies show placental abnormalities. The increase in embryonic/fetal mortality, IUGR and abnormal placental structure in (CBA/CaH \times DBA/2J) F1 IUGR placentae raised the question of whether there are also perturbations of the placenta evident for fetuses that macroscopically appear normal and have normal weight. In short, is there a predisposition in the (CBA/CaH \times DBA/2J) F1 placenta that leads to IUGR and embryonic/fetal mortality? In the normal-weight fetal population, placentae from (CBA/CaH \times DBA/2J) F1 were significantly smaller in diameter ($p < 0.0001$) and midline cross-sectional area ($p = 0.0006$) at term and significantly higher proportion of labyrinth and lower proportion of trophospongium at mid-gestation and term, when compared to (CBA/CaH \times Balb/c) F1 (Fig. 4e and Table 2). Therein while these fetuses still achieved a normal body weight there are notable differences in the morphology of their placentae which may impact placental function.

Despite having reduced total placental area and greater proportion of labyrinthine layer (Table 2), which may have suggested altered surface area for fetomaternal exchange, there was no difference in placental efficiency between the placentae of (CBA/CaH \times DBA/2J) F1 and normal-weight (CBA/CaH \times Balb/c) F1 (Table 2). At mid-gestation, but not term, the placentae from (CBA/CaH \times DBA/2J) F1 contained 55% more

	14.5 dpc			ANOVA
	CBA × Balb/c	CBA × CBA	CBA × DBA	p-value
Placentae (N)	13	31	46	
Diameter (mm)	8.30 ± 0.34	7.06 ± 0.29	6.99 ± 0.94	0.8478
Thickness (mm)	2.28 ± 0.11	2.21 ± 0.317	3.66 ± 0.04	0.1177
Area (mm ²)	19.37 ± 1.03	14.32 ± 1.94	21.52 ± 3.97	0.1541
Labyrinth (%)	51.34 ± 2.54 ^a	62.03 ± 2.67 ^{af}	39.69 ± 2.28	0.0006
Trophospongium (%)	25.64 ± 2.36	18.09 ± 1.38 ^a	41.39 ± 8.51	0.0229
Maternal decidua (%)	23.01 ± 1.37	19.88 ± 1.28	18.91 ± 10.74	0.4961
Placental efficiency (fetal/ placental weight)	1.72 ± 0.02	1.87 ± 0.16 ^{ac}	1.20 ± 0.17	0.0084
Glycogen-containing cells (% placenta)	10.84 ± 0.0	15.86 ± 1.19 ^c	9.85 ± 1.24	0.0022
	18.5 dpc			ANOVA
Placentae (N)	5	6	6	
Diameter (mm)	7.63 ± 0.28	7.36 ± 0.55	6.83 ± 0.59	0.1883
Thickness (mm)	2.42 ± 0.18	2.33 ± 0.06	2.07 ± 0.20	0.6188
Area (mm ²)	18.71 ± 2.33	15.64 ± 1.47	12.83 ± 1.55	0.1240
Labyrinth (%)	48.64 ± 2.99	64.25 ± 3.25	60.81 ± 5.11	0.0529
Trophospongium (%)	29.08 ± 4.37	19.45 ± 1.72	24.16 ± 2.39	0.0691
Maternal decidua (%)	22.29 ± 2.39	16.31 ± 2.85	18.07 ± 5.19	0.2443
Placental efficiency (fetal/ placental weight)	1.21 ± 0.27	1.82 ± 0.53	0.60 ± 0.37	0.1761
Glycogen-containing cells (% placenta)	14.14 ± 2.25	8.74 ± 0.79 ^d	9.78 ± 1.14	0.0319

Table 1. Characteristics of placentae from IUGR fetuses. Data are expressed as mean ± SEM. ^ap < 0.05, ^bp < 0.01, ^cp < 0.001 vs (CBA/CaH × DBA/2J) F1; ^dp < 0.05, ^ep < 0.01, ^fp < 0.001 vs (CBA/CaH × Balb/c) F1 by One-way ANOVA with Tukey's multiple comparison test. For each placenta two parallel sections taken 100 μm apart were analysed.

	14.5 dpc			ANOVA
	CBA × Balb/c	CBA × CBA	CBA × DBA	p-value
Placentae (N)	34	35	36	
Diameter (mm)	8.84 ± 0.35	8.85 ± 0.14	9.17 ± 0.14	0.2810
Thickness (mm)	2.67 ± 0.07	2.46 ± 0.04 ^a	2.63 ± 0.05	0.0250
Area (mm ²)	23.97 ± 1.01	22.35 ± 0.60	23.92 ± 0.69	0.1809
Labyrinth (%)	48.10 ± 1.09 ^a	54.83 ± 0.96 ^{af}	52.44 ± 0.80 ^d	0.0006
Trophospongium (%)	28.61 ± 0.61 ^a	23.46 ± 0.71 ^f	24.75 ± 0.71 ^d	0.0012
Maternal decidua (%)	23.29 ± 0.71	21.71 ± 0.83	22.81 ± 0.74	0.4442
Placental efficiency (fetal/ placental weight)	1.86 ± 0.03	2.25 ± 0.14 ^e	2.447 ± 0.36	0.0068
Glycogen-containing cells (% placenta)	10.00 ± 0.72	8.19 ± 0.53 ^c	12.68 ± 0.98	0.0004
	18.5 dpc			ANOVA
Placentae (N)	50	44	46	
Diameter (mm)	10.38 ± 0.093 ^c	9.69 ± 0.09 ^f	9.45 ± 0.15 ^f	<0.0001
Thickness (mm)	2.72 ± 0.03	2.50 ± 0.04 ^e	2.65 ± 0.04	0.0063
Area (mm ²)	26.05 ± 0.40 ^c	21.58 ± 0.50 ^f	23.22 ± 0.56 ^f	<0.0001
Labyrinth (%)	63.51 ± 0.64 ^a	48.64 ± 2.99 ^{af}	65.78 ± 0.97 ^d	<0.0001
Trophospongium (%)	19.79 ± 0.49	16.96 ± 0.52 ^c	18.82 ± 0.59	0.0088
Maternal decidua (%)	16.66 ± 0.38	14.01 ± 0.55 ^c	15.53 ± 0.68	0.0094
Placental efficiency (fetal/ placental weight)	10.00 ± 0.24	11.20 ± 0.25 ^c	10.41 ± 0.26	0.0055
Glycogen-containing cells (% placenta)	9.47 ± 0.16	8.60 ± 0.30 ^e	9.23 ± 0.38	0.0077

Table 2. Characteristics of placentae from normal-weight fetuses. Data are expressed as mean ± SEM. ^ap < 0.05, ^bp < 0.01, ^cp < 0.001 vs (CBA/CaH × DBA/2J) F1; ^dp < 0.05, ^ep < 0.01, ^fp < 0.001 vs (CBA/CaH × Balb/c) F1 by One-way ANOVA with Tukey's multiple comparison test. For each placenta two parallel sections taken 100 μm apart were analysed.

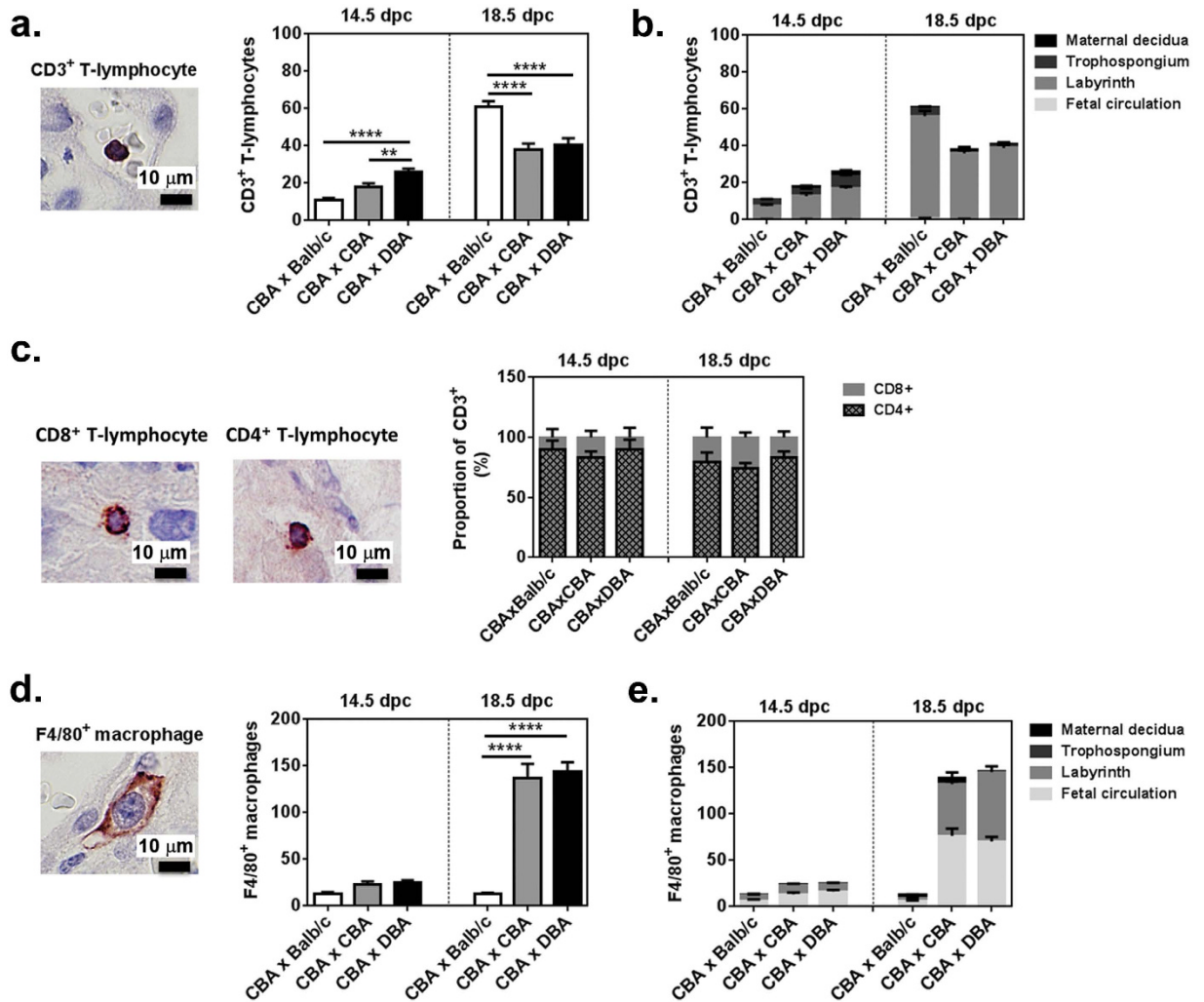


Figure 5. Inflammatory infiltrate of murine placentae from normal-weight fetuses at 14.5 and 18.5 dpc.

(a) Representative micrograph and quantitation of CD3⁺T-lymphocytes in placentae and (b) their distribution among the placental layers. (c) The proportion of CD4⁺ helper T-lymphocytes and CD8⁺ CTLs to the placental T-lymphocyte infiltrate. (d) Representative micrograph and quantitation of F4/80⁺ macrophages and (e) their distribution among the placental layers. In (a–c) micrographs from placentae of (CBA/CaH × Balb/c) F1 fetuses at 18.5 dpc are shown to demonstrate positive staining of the immune cell types. Data are represented as mean ± SEM. N = 34–50 placentae/strain/dpc as outlined in Table 2. **p < 0.01, ****p < 0.0001, as indicated by One-way ANOVA with Tukey’s multiple comparison test.

glycogen-containing cells compared to placentae from (CBA/CaH × CBA/CaH) F1 (p = 0.0009) and 27% more than (CBA/CaH × Balb/c) F1 (p = 0.09; Fig. 4e and Table 2). Placentae from (CBA/CaH × CBA/CaH) F1 had the lowest proportion of glycogen-containing cells at both 14.5 (8.19 ± 0.53%) and 18.5 dpc (8.60 ± 0.29%; Table 2), consistent with the lowest placental weights for normal-weight fetuses (Fig. 4b). Whether these differences in glycogen-storage are causal for reduced fetal growth or compensatory is unclear.

A hallmark of placentae from IUGR pregnancies is marked inflammatory infiltrate¹¹. While macrophages and T-lymphocytes are required for normal placentation, excessive and/or prolonged inflammation contributes to the pathology of IUGR by damaging the fetal-maternal interface, promoting trophoblast cell death^{9,10,27}. At mid-gestation placentae from (CBA/CaH × DBA/2J) F1 normal-weight fetuses contained significantly more CD3⁺ T-lymphocytes than (CBA/CaH × CBA/CaH) F1 (1.4-fold, p < 0.01) or (CBA/CaH × Balb/c) F1 placentae (2.6-fold, p < 0.0001; Fig. 5a). While the absolute number of CD3⁺ T-lymphocytes was higher in all groups at term, intriguingly there was 1.5-fold more CD3⁺ T-lymphocytes in (CBA/CaH × Balb/c) F1 placentae than (CBA/CaH × CBA/CaH) F1 and (CBA/CaH × DBA/2J) F1 placentae (both p < 0.0001). In all groups and time points >85% of CD3⁺ T-lymphocytes localised to the labyrinth (Fig. 5b). Subsequent analysis for CD4⁺ helper T-lymphocytes and CD8⁺ CTLs showed that while the absolute number of CD3⁺ T-lymphocytes differed among the groups, the proportion of CD4⁺ helper vs CD8⁺ CTLs was not significantly different; >83% CD4⁺ helper T-lymphocytes at mid gestation and >74% at term (Fig. 5c).

Two populations of F4/80⁺ macrophages are present in placenta; maternal haematopoietic-derived macrophages and fetal yolk sac-derived macrophages (Hofbauer cells)²⁸. In addition to differences in origin, fetal macrophages predominantly localise to the chorionic villi (labyrinth in mice) and fetal circulation, and maternal macrophages to the maternal decidua²⁸. (CBA/CaH × DBA/2J) F1 placentae had 1.8-fold more F4/80⁺ macrophages than (CBA/CaH × Balb/c) F1 placentae at mid-term and 11-fold more at term (Fig. 5d). These changes were also mimicked in (CBA/CaH × CBA/CaH) F1. Within the placentae, 30–50% of macrophages localised to labyrinth and 50–70% to the fetal circulation (chorionic plate; Fig. 5e). Our data shows that there is altered temporal and spatial distribution of T-lymphocyte and macrophages even in the placentae (CBA/CaH × DBA/2J) F1 fetuses that achieve a normal-weight.

Discussion

The data in this study demonstrates that the IUGR and embryonic/fetal mortality phenotype of the CBA/J × DBA/2J model can also be elicited by using the Commonwealth-derived CBA/CaH substrain. First, prevalence of IUGR and mortality was higher at 14.5 dpc in (CBA/CaH × DBA/2J) F1 than (CBA/CaH × Balb/c) F1. Second, in all strains IUGR fetuses were associated with lighter, smaller placentae with histopathology and reduced materno-fetal exchange as evidenced by smaller labyrinth and lower placental efficiencies when compared to normal-weight fetuses of the same strain. Finally, despite some fetuses obtaining 'normal' body weight, the placentae from these (CBA/CaH × DBA/2J) F1 show altered glycogen storage and considerable T-lymphocyte and macrophage inflammatory infiltration compared to (CBA/CaH × Balb/c) F1. These findings suggest that there is a range of placental pathology in the CBA/CaH × DBA/2J pregnancy which dictates the fetal outcome; severe pathology leads to early resorption, moderate to IUGR at 14.5 dpc with subsequent demise by term, and mild which supports live birth.

Among inbred murine strains there is a spectrum of gestational lengths, fetal and placental weights, maternal weight gain and number of concepti²⁹. While gestational length and concepti are largely dependent upon maternal genotype²⁹, which was unchanged in our study, fetal and placental weight are dependent on the genetic composition of the embryo. Of our three inbred strains, the syngeneic (CBA/CaH × CBA/CaH) F1 had the lowest fetal and placental weights of our normal-weight cohorts, consistent with the 14–20% lower fetal and placental weight reported in allogeneic *vs* syngeneic inbred matings^{30–32}. The acquirement of heterosis in F1 fetuses is shown to precede implantation, with blastocysts of syngeneic pregnancies containing more cells than allogeneic pregnancies at the same gestational age³³. As placentation continues the mixed genetic background of the fetuses may become more influential with differences in remodelling of the uterine vasculature and maternal immunological response associated with paternal MHC expression³⁴. Yet, precisely how the mixed genetic background of (CBA/CaH × DBA/2J) F1 fetuses leads some to achieve normal-weight while others are growth restricted or die is unknown.

Technological advancements and greater appreciation of the placenta as an immunomodulatory organ have provided increasing evidence that dysregulation of placentation, and not a loss of maternal immune tolerance against the semi-allogeneic fetus *per se*, underlie human and murine (CBA/J × DB/2JA) IUGR and mortality^{8–10,35}. Following implantation fetal trophoblasts invade the maternal decidua and partner resident natural killer (NK) cells³⁶ to remodel spiral arteries by inducing apoptosis of endothelial cells and vascular smooth muscle cells by soluble Fas ligand^{37–39} and tumour necrosis factor- α -related apoptosis-inducing ligand. Apoptotic cells are phagocytosed, typically by decidual macrophages, though first trimester trophoblasts are phagocytic⁴⁰ and may also play a role in clearing these cells during spiral artery remodelling. Such aberrations in the function of the trophoblasts or NK cells results in a failure to convert the maternal spiral arteries into low resistance, high capacity vessels³⁹. Subsequent perfusion of the placenta with maternal blood at high pressure incites trophoblast damage via shear stress and mechanical damage⁴¹ leading to thrombotic and fibrotic events as noted in the IUGR placentae of all murine strains in our study, and infarcts, loss of tertiary villi and increased syncytial knots (associated with syncytiotrophoblast apoptosis) among the placentae of human IUGR newborns⁴². Such injury to the human placental villi or murine labyrinth reduces the surface area of materno-fetal exchange contributing to IUGR.

Delineation of the initial mechanism that renders trophoblasts or decidual NK cells less effective at spiral artery remodelling is a relatively new field of research and is complicated by access to very early human placental tissue and the differences between invasiveness of murine and human trophoblasts. From the CBA/J × DBA/2J model there is evidence of inadequate placentation via poor maternal arterial remodelling at the implantation sites⁵ and perturbations of genomic DNA methylation in the maternal decidua⁴³. Other studies report inflammatory mechanisms, with complement deposition on trophoblasts with increased neutrophil and monocyte infiltration and TNF- α expression in maternal decidua and reduced trophoblast giant cells in placentae of resorbing fetuses⁶. Both abnormal DNA methylation and complement deposition appear to distinguish normally developing fetuses from those which resorb, even within the same litter^{6,43}. Our study compliments this evidence wherein perturbations in placental size and morphology were observed in placentae of IUGR fetuses when compared to normal-weight littermates. In humans, these parameters dictate the number of maternal spiral arteries that can be remodelled and subsequently influences the surface area of nutrient exchange in the placenta⁴⁴ affecting fetal growth and development.

It is understandable that the outcome of any fetus is dependent on the severity of impact to the placenta, as the key regulator of both oxygen and nutrients. Mild alterations in placental morphology or inflammation below a threshold do not observably impact on weight or CRL but may evoke epigenetic or anatomical changes that alter ongoing fetal-adult development. To our knowledge the CBA × DBA model has not been examined as far as pup development following birth, largely due to the need to excise uteri and fetuses for assessment of embryonic/fetal mortality and IUGR. However, as ultrasound biomicroscopy technology becomes more cost-effective, such non-invasive assessments of viable *vs* non-viable murine fetuses on the basis of heart beat⁴⁵, as well as *in situ*

murine fetal growth measurements⁴⁶ will be reported and enable long term outcomes to be assessed in this model. Of particular note would be cognitive function and behavioural impacts as these are commonly associated with children who were IUGR⁴⁷, despite ‘catching up’ in weight after birth. This will be essential for assessment of novel therapeutics to reduce embryonic/fetal mortality and IUGR using the CBA × DBA/2J model.

In summary, we have provided a comprehensive assessment of fetal outcome and placental dimension and immune infiltrate temporal and spatial anomalies at two gestational time points (14.5 and 18.5 dpc), with both allogeneic and syngeneic control matings, to demonstrate that the CBA/CaH × DBA/J is an equivalent murine model of IUGR and embryonic/fetal mortality to the CBA/J × DBA/2J model for assessment of pregnancy pathology and/or novel therapeutics.

Methods

Animals and Tissue Preparation. All experiments were approved and performed in accordance with the guidelines of the Northern Sydney Local Health District Animal Research Ethics Committee, Australia (ACEC 1311-015A). Twelve-week old virgin female CBA/CaH.Arc and male CBA/CaH.Arc (*H2k*), Balb/c.Arc (*H2d*), and DBA/2J.Arc (*H2d*) mice were purchased from the Animal Resources Centre (Murdoch, Australia). Animals were provided food and water *ad libitum* and kept under specific pathogen-free conditions with controlled humidity and light conditions.

Timed syngeneic CBA/CaH × CBA/CaH, and allogeneic CBA/CaH × Balb/c or CBA/CaH × DBA/2J matings were performed by pairing females with males overnight. Detection of the vaginal plug denoted 0.5 days post coitum (dpc). At 14.5 dpc (mid-gestation; N = 20 dams per strain) and 18.5 dpc (term; N = 30 dams per strain) pregnant mice were sacrificed by cervical dislocation and the gravid uteri, including the cervix, were harvested and weighed. Subsequently, each fetus and placenta were dissected, weighed, the fetal crown-rump length measured, and the litter photographed. The number of concepti and embryonic/fetal mortality (resorption) rate were also recorded. Embryonic/fetal mortality was defined as including ‘macerated pale fetuses (embryonic)’, bag of cells, and ‘clot’¹⁸. Pink/perfused fetuses were considered viable. Overall there was ≥80% pregnancy success in each group. In the term population, two pregnant dams from each group delivered pre-term at 17.5 dpc and were excluded from subsequent analyses.

Histology and Immunohistochemistry. *Paraffin-embedded tissues.* Four μm sections of paraffin-embedded resorptions and placentae were cut sagittal to the midline and stained with haematoxylin and eosin (general morphology), periodic acid Schiff’s (PAS) procedure (glycogen-positive cells in the trophospongium), or fast-green Masson’s trichrome stain (fibrosis). Immunohistochemistry was performed for T-lymphocytes (CD3e; 1 μg/ml DAKO) and monocyte/macrophages (F4/80; 2 μg/ml Santa Cruz) following proteinase K (2 mg/ml) antigen retrieval. Normal rat and rabbit IgG served as isotype controls (DAKO).

Frozen tissues. Resorptions and placentae snap-frozen in liquid nitrogen were embedded in Optimal Cutting Temperature compound. Eight μm cryosections were immunohistochemically stained for helper T-lymphocytes (CD4; 0.5 μg/ml Santa Cruz) and cytotoxic T-lymphocytes, CTL (CD8; 0.5 μg/ml Santa Cruz). Normal rat IgG served as isotype control (DAKO).

Placental Structure Quantification. Quantitation of the placental dimensions (diameter, thickness, and midline cross-sectional area) were analysed using haematoxylin and eosin stained sections and the placental layers (labyrinth, trophospongium and maternal decidua) using PAS-stained sections. All histological analyses were performed using two parallel sections per IUGR and normal-weight placentae taken at least 100 μm apart. Low magnification micrographs were taken using a Nikon Eclipse Ci microscope fitted with a DS-Fi1 digital camera and DS-U2 control unit and 2x Plan Achromat objective lenses. From the scale bar placental diameter, thickness, and midline cross-sectional area were measured using ImageJ 1.48v software (<http://imagej.nih.gov/ij>) and expressed in millimetres. The area attributed to the labyrinth, trophospongium and maternal decidua layers was assessed and expressed as a percentage of the total area of the placenta (excluding fetal circulation structures). The percentage of glycogen-containing trophoblasts in PAS-stained sections was quantified by magenta-coloured pixels in micrographs using ImageJ 1.48v software (<http://imagej.nih.gov/ij>). A macro to automate the analysis was modified from the freely available ImageJ resource at <http://imagej.net/docs/examples/stained-sections/index.html> (NIH) and utilised the green channel and a magenta colour threshold of (0, max/1.4). For each section the data was calculated as the area of magenta coloured pixels/placental midline cross-sectional area*100 and expressed as glycogen-containing cells as a proportion (%) of the placental area.

Statistical Analyses. Normality of the data for each outcome was determined by the D’Agostino & Pearson omnibus K2 normality test (GraphPad Prism; NIH), except the IUGR 18.5 dpc cohorts due to low sample size (normal distribution was assumed using the Central Limit Theorem as the placentae are derived from normally distributed populations; see Fig. 3b). Data are expressed as mean ± standard error of the mean (SEM). Comparison between groups at 14.5 dpc and 18.5 dpc was performed using unpaired two-tailed Student t-test and between groups of a single time point by One-way ANOVA with Tukey’s multiple comparison test. Association between crown-rump length and fetal weight was determined by Pearson correlation. The Chi square test was used to compare the number of concepti between left vs right uterine horns, the frequency of perinatal mortality in ‘crowded’ vs ‘uncrowded’ horns, incidence of placentally-fused twins, and differences in proportion of litters with resorbing fetuses vs those without. A p-value < 0.05 was considered statistically significant for all analyses.

References

1. WHO. *Expert Committee Report: Physical status: the use and interpretation of anthropometry*. (World Health Organization, 1995).
2. Baschat, A. Fetal responses to placental insufficiency: an update. *Br. J. Obstet. Gynaecol.* **111**, 1031–1041 (2004).
3. Alexander, G. *et al.* US birth weight/gestational age-specific neonatal mortality: 1995–1997 rates for whites, hispanics, and blacks. *Pediatrics.* **111**, e61–e66 (2003).
4. Ott, W. An update on the ultrasonic diagnosis and evaluation of intrauterine growth restriction. *Ultrasound Rev. Obstet. Gynecol.* **5**, 111–124 (2005).
5. Clark, D. A., McDermott, M. R. & Szewczuk, M. R. Impairment of host-versus-graft reaction in pregnant mice: II. Selective suppression of cytotoxic T-cell generation correlates with soluble suppressor activity and with successful allogeneic pregnancy. *Cell. Immunol.* **52**, 106–118 (1980).
6. Girardi, G., Yarilin, D., Thurman, J., Holers, V. & Salmon, J. E. Complement activation induces dysregulation of angiogenic factors and causes fetal rejection and growth restriction. *J. Exp. Med.* **203**, 2165–2175 (2006).
7. Ahmed, A., Singh, J., Khan, Y., Seshan, S. & Girardi, G. A new mouse model to explore therapies for preeclampsia. *PLoS One.* **5**, e13663 (2010).
8. Dixon, M. E., Chien, E. K., Osol, G., Callas, P. W. & Bonney, E. A. Failure of decidual arteriolar remodeling in the CBA/J × DBA/2 murine model of recurrent pregnancy loss is linked to increased expression of tissue inhibitor of metalloproteinase 2 (TIMP-2). *Am. J. Obstet. Gynecol.* **194**, 113–119 (2006).
9. Whitley, G. S. J. & Cartwright, J. E. Trophoblast-mediated spiral artery remodelling: a role for apoptosis. *J. Anat.* **215**, 21–26 (2009).
10. Scifres, C. M. & Nelson, D. M. Intrauterine growth restriction, human placental development and trophoblast cell death. *J. Physiol.* **587**, 3453–3458 (2009).
11. Mestan, K. *et al.* Placental inflammatory response is associated with poor neonatal growth: preterm birth cohort study. *Pediatrics.* **125**, e891–e898 (2010).
12. Chaouat, G. *The immunology of the fetus*. 254–259 (CRC Press, 1990).
13. Bobe, P. & Kiger, N. Immunogenetic studies of spontaneous abortion in mice. III. Non-H-2 antigens and gestation. *J. Immunogenet.* **16**, 223–231 (1989).
14. Click, R. & Adelman, A. Multi-gene/allele control of Mlsb of CBA/H. *Immunogenetics.* **29**, 155–160 (1989).
15. Qing, X. *et al.* Targeted inhibition of complement activation prevents features of preeclampsia in mice. *Kidney Int.* **79**, 331–339 (2001).
16. Poudel, R. *et al.* Effects of 2-methoxyestradiol administration in mouse models purported to show signs of preeclampsia and fetal growth restriction. *Int. J. Reprod. Fertility & Sex. Health* (2014).
17. Ohlemiller, K. K., Dahl, A. R. & Gagnon, P. M. Divergent Aging Characteristics in CBA/J and CBA/CaJ Mouse Cochleae. *Journal of the Association for Research in Otolaryngology.* **11**, 605–623 (2010).
18. Milliam Stanley, M. & Solderwall, A. Morphological changes accompanying fetal resorption in the Golden Hamster. *Am. J. Anat.* **114**, 539–549 (1964).
19. Chavez, D. J., McIntyre, J. A., Colliver, J. A. & Faulk, W. P. Allogeneic matings and immunization have different effects on nulliparous and multiparous mice. *J. Immunol.* **139**, 85–88 (1987).
20. Ho, H. *et al.* Age, environment, and lymphocyte immunization influence the spontaneous resorption rate in the CBA/J × DBA/2J mouse model. *Am. J. Reprod. Immunol.* **31**, 47–51 (1994).
21. Rocha, F. & Zalud, I. In *Donald School Textbook of Ultrasound in Obstetrics and Gynecology* (eds Kurjak, A. & Chervenak, F. A.) Ch. 14, 213 (Jaypee Brothers Medical Publishers (P) Ltd, 2011).
22. Levi, M., Manahan, J. & Mandi, I. Specific resorption of the mouse fetus. *Obstet. Gynecol.* **33**, 11–19 (1969).
23. England, G. C. W. & Russo, M. Ultrasonographic characteristics of early pregnancy failure in bitches. *Theriogenology.* **66**, 1694–1698 (2006).
24. Kotgirwar, S., Ambiyee, M., Athavale, S., Gupta, V. & Trivedi, S. Study of gross and histological features of placenta in intrauterine growth retardation. *J. Anat. Soc. India.* **60**, 37–40 (2011).
25. Biswas, S. Placental changes in idiopathic intrauterine growth restriction. *OA Anatomy.* **1**, 11 (2013).
26. Wilson, M. & Ford, S. Comparative aspects of placental efficiency. *Reprod. Suppl.* **58**, 223–232 (2001).
27. Cotechini, T. *et al.* Inflammation in rat pregnancy inhibits spiral artery remodeling leading to fetal growth restriction and features of preeclampsia. *J. Exp. Med.* **211**, 165–179 (2014).
28. Pinhal-Enfield, G., Vasan, N. & Leibovich, S. In *Embryology - Updates and Highlights on Classic Topics* (ed. Pereira, L. V.) Ch. 6, 127–142 (InTech, 2012).
29. Murray, S. A. *et al.* Mouse gestation length is genetically determined. *PLoS One.* **5**, e12418 (2010).
30. McCarthy, J. C. Genetic and environmental control of foetal and placental growth in the mouse. *Animal Science.* **7**, 347–361 (1965).
31. McLaren, A. Genetic and environmental effects on foetal and placental growth. *J. Reprod. Fertil.* **9**, 79–98 (1965).
32. Hetherington, C. M. The decidual cell reaction, placental weight, foetal weight and placental morphology in the mouse. *J. Reprod. Fertil.* **25**, 417–424 (1971).
33. Gates, A., Doyle, L. & Noyes, R. A physiological basis for heterosis in hybrid mouse fetuses. *Amer. Zool.* **1**, 449 (1961).
34. Madeja, Z. *et al.* Paternal MHC expression on mouse trophoblast affects uterine vascularization and fetal growth. *Proceedings of the National Academy of Sciences of the United States of America.* **108**, 4012–4017 (2011).
35. Chaouat, G. *et al.* An insight into normal and pathological pregnancies using large-scale microarrays: lessons from microarrays. *J. Reprod. Immunol.* **89**, 163–172 (2011).
36. Wallace, A. E., Fraser, R. & Cartwright, J. E. Extravillous trophoblast and decidual natural killer cells: a remodelling partnership. *Hum. Reprod. Update.* **18**, 458–471 (2012).
37. Ashton, S. V. *et al.* Uterine spiral artery remodeling involves endothelial apoptosis induced by extravillous trophoblasts through Fas/FasL interactions. *Arterioscler. Thromb. Vasc. Biol.* **25**, 102–108 (2005).
38. Harris, L. K. *et al.* Invasive trophoblasts stimulate vascular smooth muscle cell apoptosis by a fas ligand-dependent mechanism. *Am. J. Pathol.* **169**, 1863–1874 (2006).
39. Fraser, R. *et al.* Impaired decidual natural killer cell regulation of vascular remodelling in early human pregnancies with high uterine artery resistance. *J. Pathol.* **228**, 322–332 (2012).
40. Choy, M. Y. & Manyonda, I. T. The phagocytic activity of human first trimester extravillous trophoblast. *Human reproduction (Oxford, England).* **13**, 2941–2949 (1998).
41. Burton, G. J., Woods, A. W., Jauniaux, E. & Kingdom, J. C. Rheological and physiological consequences of conversion of the maternal spiral arteries for uteroplacental blood flow during human pregnancy. *Placenta.* **30**, 473–482 (2009).
42. Veerbeek, J. H. *et al.* Placental pathology in early intrauterine growth restriction associated with maternal hypertension. *Placenta.* **35**, 696–701 (2014).
43. Brown, L. Y., Bonney, E. A., Raj, R. S., Nielsen, B. & Brown, S. Generalized Disturbance of DNA Methylation in the Uterine Decidua in the CBA/J × DBA/2 Mouse Model of Pregnancy Failure. *Biol. Reprod.* **89**, 120 (2013).
44. Salafia, C., Charles, A. & Maas, E. Placenta and fetal growth restriction. *Clin. Obstet. Gynaec.* **49**, 236–256 (2006).
45. Flores, L. E., Hildebrandt, T. B., Kühl, A. A. & Drews, B. Early detection and staging of spontaneous embryo resorption by ultrasound biomicroscopy in murine pregnancy. *Reprod. Biol. Endocrinol.* **12**, 38–38 (2014).

46. Mu, J., Slevin, J. C., Qu, D., McCormick, S. & Adamson, S. L. *In vivo* quantification of embryonic and placental growth during gestation in mice using micro-ultrasound. *Reprod. Biol. Endocrinol.* **6**, 34 (2008).
47. Geva, R., Eshel, R., Leitner, Y., Valevski, A. & Harel, S. Neuropsychological outcome of children with intrauterine growth restriction: A 9-year prospective study. *Pediatrics.* **118**, 91–100 (2006).

Acknowledgements

K.J.M.'s work is supported by the National Health & Medical Research Council (NHMRC), Australia (CIA JMM, grant number GNT1066606, 2014); and S.A.M.'s by Ramsay Health Care, Australia.

Author Contributions

S.A.M., J.M.M. and A.W.A. conceived the project and provided input on data analysis and interpretation of the experimental findings, V.M.Y. and K.J.M. performed mouse matings, K.J.M. performed data analyses, wrote the manuscript and prepared the figures. All authors reviewed the manuscript.

Additional Information

Supplementary information accompanies this paper at <http://www.nature.com/srep>

Competing financial interests: The authors declare no competing financial interests.

How to cite this article: McKelvey, K. J. *et al.* Embryonic/fetal mortality and intrauterine growth restriction is not exclusive to the CBA/J sub-strain in the CBA × DBA model. *Sci. Rep.* **6**, 35138; doi: 10.1038/srep35138 (2016).



This work is licensed under a Creative Commons Attribution 4.0 International License. The images or other third party material in this article are included in the article's Creative Commons license, unless indicated otherwise in the credit line; if the material is not included under the Creative Commons license, users will need to obtain permission from the license holder to reproduce the material. To view a copy of this license, visit <http://creativecommons.org/licenses/by/4.0/>

© The Author(s) 2016